Journal of Materials Chemistry A

Accepted Manuscript

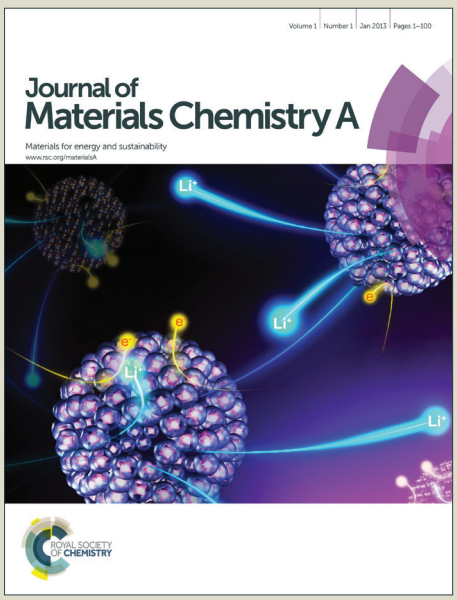

ROYAL SOCIETY OF CHEMISTRY

www.rsc.org/materialsA

Journal Name

ARTICLE

Hierarchical hybrid nanostructures of Sn_3O_4 on N doped TiO_2 nanotubes with enhanced photocatalytic performances

Received 00th January 20xx,
Accepted 00th January 20xx

DOI: 10.1039/x0xx00000x

www.rsc.org/

Xin Yu,[ab1] Longfei Wang,[ab1] Jian Zhang,[ab] Weibo Guo,[ab] Zhenhuan Zhao,[c] Yong Qin,[a] Xiaoning Mou,[a] Aixue Li[a]* and Hong Liu[ac]*

Semiconductor nanostructures with photocatalytic activity have many potential applications including remediation of environmental pollutants and photocatalytic hydrogen evolution. An effective way for promoting photocatalytic activity is creating heterogeneous photcatalysts. In this paper, a hybrid nanostructured photocatalyst with desired three-dimensional (3D) nanoarchitectures by assembling Sn_3O_4 nanosheets on N-doped TiO_2 nanotubes has been constructed with enhanced broad spectrum photocatalytic properties, which can harness UV, visible light to decompose organic contaminants in aqueous solution and split water to hydrogen. Photocatalytic tests displayed that the Sn_3O_4/N-TiO_2 hierarchical hybrid nanostructures possessed a much higher degradation rate of methyl orange and hydrogen evolution rate than that of the unmodified TiO_2 nanotubes, N-TiO_2 nanotubes, Sn_3O_4 nanosheets and Sn_3O_4/TiO_2 hybrid nanostructures. The mechanism related to the enhancement of photocatalytic activity was discussed. Deposition of Sn_3O_4 nanosheets onto N-TiO_2 nanotubes resulted in a dramatic increase in light-induced generation of hydroxyl radical, superoxide and singlet oxygen, and production of holes and electrons. This work is the first instance of combining Sn_3O_4 with N-TiO_2, the Sn_3O_4/N-TiO_2 hierarchical hybrid nanostructures shows good photocatalytic performance. This study is potentially applicable to a range of 3D hybrid nanostructures with promising applications in photocatalysis and relevant areas.

Introduction

In modern society, the technology of semiconductor-based photocatalytic for degradating environmental pollutants and splitting water to produce hydrogen by taking advantage of solar energy has been considered as one of the most important approaches to solving the world energy crisis.[1] Hence, the development of the necessary semiconductor photocatalysts has undergone considerable research.[2] Titanium dioxide (TiO_2) has been widely investigated as a photoanode for photodegradation and water splitting because of its favorable band-edge position, strong optical absorption, superior chemical stability and anti-photocorrosion, biocompatibility[3] and low cost.[4-5] However, pure TiO_2 can only absorb ultraviolet light which accounts for only about 4% of the energy of the sunlight, due to its large bandgap (3.2 eV for anatase), which greatly impedes its widespread applications.[6, 7] Therefore, developing highly active photocatalysts coupled with efficient photocatalysis techniques is valuable.[8]

Now, many methods have been developed to pursue highly active photocatalysts: first, reducing the band gap of photocatalysts to the visible light region through bandgap engineering including metal and non-metal doping in semiconductors to broaden the absorption from UV region to visible light region.[9] In particular, due to the compatible size to oxygen and small formation energy required for the substitution of Ni, N, V, Co, they has been widely used as the dopant to modify the electronic structures of oxide semiconductors.[10, 11, 12, 13] Second, exploring novel kinds of photocatalysts with narrow bandgap in which Sn_3O_4 has been experimentally confirmed to possess absorption bands in visible-light region, attracted a great deal of attention for its good photocatalytic performance in energy conversion[14] and remediation[15] under visible light irradiation, which accounts for about 48% of the incoming solar energy, due to the comprehensive understanding of heterovalent semiconductor oxides. Third, constructing hybrid nanomaterials with different semiconductor or semiconductor/metal nanoparticles is demonstrated as an efficient way for promoting photo-induced carrier separation based on p-n heterojunction,[16] Schottky heterojuction[17] and band structure matching physical mechanism.[18]

In recent years, nanostructured materials have attracted considerable attention for photocatalysis due to their unique physical and chemical properties compared to their bulk counterparts.[19] These diverse nanostructures such as nanoparticles,[20] nanoporous,[21] nanospheres,[22] nanobelts,[23] nanorods,[24] nanowires[25] and other more complex structures[26] have been demonstrated to show extraordinary unconventional properties, which can greatly enrich the material selection and

[a] Beijing Institute of Nanoenergy and Nanosystems, Chinese Academy of Science, Beijing 100083, China
[b] University of Chinese Academy of Science, Beijing 100049, China
[c] State Key Laboratory of Crystal Materials, Shandong University, Jinan 250100, China
Xin Yu and Longfei Wang are contributed equally to this work.
† Footnotes relating to the title and/or authors should appear here.
Electronic Supplementary Information (ESI) available: [details of any supplementary information available should be included here]. See DOI: 10.1039/x0xx00000x

open a new degree of freedom for the design of effective photocatalytic systems.[27] Meanwhile, the availability of a broad range of nanostructures can allow for flexible integration of multiple functional components to create heterogeneous structures with unique characteristics or unprecedented performance.[28, 29] Recently, TiO_2-based materials nanocomposites have attracted a great deal of research attention.[30] And its main purposes are to broaden spectrum absorption and to promote the separation of the photocarriers using the heterostructures. The TiO_2-based nanocomposites are mainly about particulate, film-like and fibrous (or banded) structures.[7] However, TiO_2 nanoparticles composite is easy to from unexpected formation (a core-shell structure) that blocks UV light absorption and restricts the diffusion of photoinduced charge carriers to the composite surface.[31] Although the film-like composite can realize UV and visible light photocatalysis by adjusting the density of the secondary phase material, the film is a two dimensional (2D) structure, so the unit mass photocatalytic performance is very low. Recent studies show that TiO_2 nanobelt has been studied extensively.[32] In comparison with nanoparticles and films, TiO_2 nanobelt composites are displayed new properties and can improve the UV-visible photocatalytic performance.[33] However, it is difficult to achieve mass preparation due to the complex synthesis method. TiO_2 nanotubes synthesis by electrospinning method which can overcome the problem.[34] Furthermore, it is a polycrystalline nanotube consisted of nanoparticles, so it has a large active surface. More importantly, the mutual connection between these particles is conducive to photocarrier transport. At the same time, due to the nanotube structure, the catalytic active site is not limited to the surface of the nanotubes, also can be realized in the tube cavity. Moreover, it is more appropriate to build flexible photocatalytic system using the TiO_2 nanotube.

Inspired by the correlation between shape/morphology and performances of photocatalysts, we reported a discovery of a novel photocatalyst of desired 3-D nanoarchitectures by assembling Sn_3O_4 nanosheets on N-doped TiO_2 nanotubes, a hybrid nanostructured photocatalyst with enhanced broad spectrum photocatalytic properties has been constructed, which can harness UV, visible light to decompose organic contaminants in aqueous solution and catalyse water splitting. An investigation of the material's photocatalytic abilities indicates that the Sn_3O_4/N-TiO_2 hierarchical hybrid nanostructures exhibit an enhanced photocatalytic activity in the decomposition of MO and promote hydrogen evolution from water solution under UV and visible light irradiation. Furthermore, these Sn_3O_4/N-TiO_2 hierarchical hybrid nanostructures can be easily recycled without a decrease in the photocatalytic activity due to their 3D nanostructured nature. It is expected that the Sn_3O_4/N-TiO_2 hierarchical hybrid nanostructures with high photocatalytic activities will greatly promote their practical application on eliminating organic pollutants from waste water and producing hydrogen.

Results and discussion

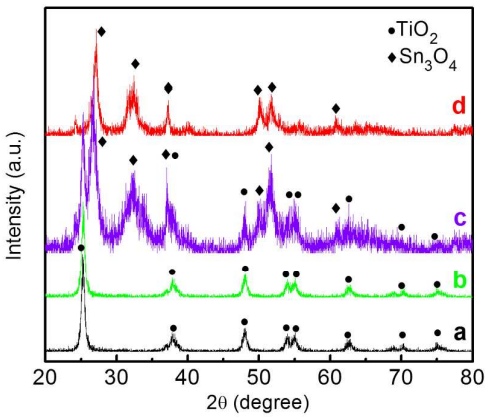

Fig. 1 XRD patterns of TiO_2 nanotubes (Curve a), N-TiO_2 nanotubes (Curve b), Sn_3O_4/N-TiO_2 hierarchical hybrid nanostructures (Curve c); Sn_3O_4 nanosheets (Curve d).X-Ray diffraction (XRD) analysis was employed to investigate the crystal phase of TiO_2 nanotubes, N-TiO_2 nanotubes, Sn_3O_4 nanosheets and Sn_3O_4/N-TiO_2 hierarchical hybrid nanostructures.

As shown in Fig. 1, all the diffraction peaks of the TiO_2 (Curve a) and N-TiO_2 (Curve b) matched these of anatase (PDF-#21-1272)[35] meanwhile those of Sn_3O_4 (Curve c) matched this of (PDF-#16-0737).[15] Otherwise, besides TiO_2, no other nitrogen-containing compounds or other titanic polymorphs were detected in the N-TiO_2 nanotubes (Curve b). Furthermore, there was no evident shift of the XRD peaks indexed to anatase phase after nitrogen doping. Thus, it is inferred that the crystalline of the anatase TiO_2 doesn't decrease after nitrogen doping. For Sn_3O_4/N-TiO_2 (Curve c) and Sn_3O_4/TiO_2 (Fig. S1) hierarchical hybrid nanomaterials, all the diffraction peaks can be well indexed to either N-TiO_2 or Sn_3O_4, indicating the nanomaterials are the compounds of Sn_3O_4/ N-TiO_2.

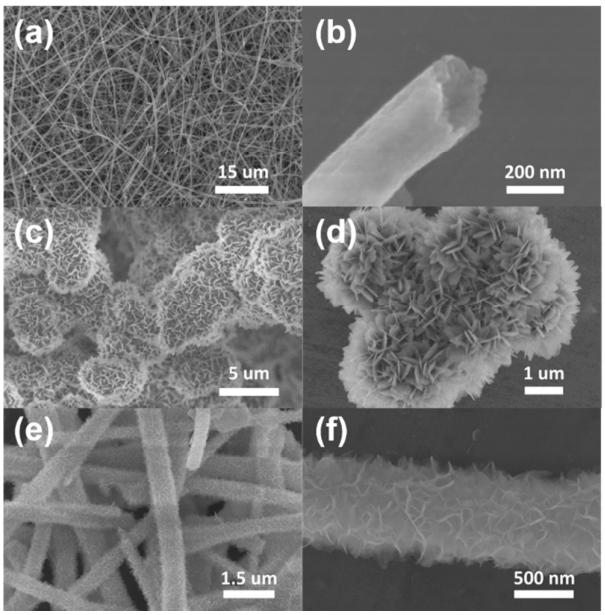

Fig. 2 SEM images of sample (a, b) N-TiO_2 nanotubes (c, d) Sn_3O_4 nanosheets (e, f) Sn_3O_4/N-TiO_2 hierarchical hybrid nanostructures.

The morphology of the as-prepared N-TiO_2 nanotubes, Sn_3O_4 nanosheets, and Sn_3O_4/N-TiO_2 hierarchical hybrid nanostructures were characterized by scanning electron microscopy (SEM). The N-TiO_2 showed a good uniformity and a relative smooth surface without secondary nanostructures from Fig. 2a. The diameter of the nanotubes ranged from 200 to 300 nm, and the length of the nanotubes range to several hundreds of micron. As shown in Fig. S2, the morphology of the nanotubes had no any visible change after nitrogen doping comparing to the TiO_2 nanotubes. Fig. 2b showed an amplified image of the N-TiO_2 nanotubes. We can clearly see the inner diameter was about 200 nm, and the wall thickness was about 20 nm. As shown in Fig. 2c, the low magnification SEM images indicated that the product of Sn_3O_4 consists of a wealth of 3-D flower-like microstructures with a diameter of 3-4 μm, while the high magnification image (Fig. 2d) showed that each flower was composed of a large quantity of nanopetals with smooth surface. Fig. 2e shows a typical SEM image of the as-synthesized Sn_3O_4/N-TiO_2 hierarchical hybrid nanostructures, where the N-TiO_2 nanotubes are uniformly decorated with Sn_3O_4 nanosheets. The nanosheets are evenly distributed over the entire surface of each nanotubes and connected to each other, forming a network of relief features on the rough surface of each nanotube. From Fig. 2f, it is easy to observe that the Sn_3O_4 nanosheets are in fact very thin flakes with an average thickness of about 8 nm and an average edge length of about 100-150nm.

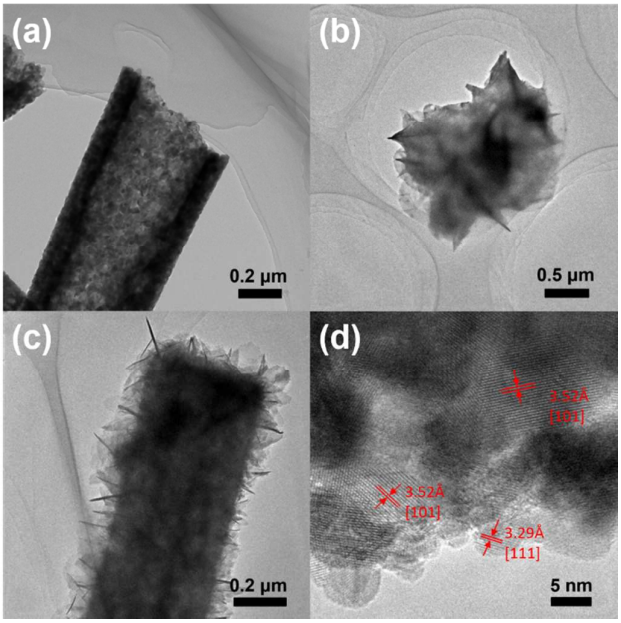

Fig. 3 TEM images of (a) N-TiO_2 nanotube (b) Sn_3O_4 nanosheets (c) Sn_3O_4/N-TiO_2 hierarchical hybrid nanostructures (d) HRTEM image of Sn_3O_4/N-TiO_2 hierarchical hybrid nanostructures.

Fig. 3 a, b and c shows the typical transmission electron microscopic (TEM) images of N-TiO_2 nanotubes, Sn_3O_4 nanosheets and Sn_3O_4/N-TiO_2 hierarchical hybrid nanostructures. The Sn_3O_4 nanosheets had a narrow size distribution. They possessed size around 50 nm, coinciding with the results from the SEM observations. As shown in Fig. 3d, the HRTEM image of the Sn_3O_4/N-TiO_2 hybrid nanostructures clearly displayed two types of lattice fringes. One set of the lattice spacing is about 0.352 nm, corresponding to the [101] crystal orientation of the anatase TiO_2.[36] Another set of the lattice spacing is about 0.329 nm, corresponding to the [111] crystal orientation of Sn_3O_4. The selected area electron diffraction (SAED) pattern (Fig. S4d) of a single nanosheet clearly demonstrated the high crystallinity of the nanosheet. The TEM image of the Sn_3O_4/N-TiO_2 hybrid nanostructure revealed that highly dense Sn_3O_4 nanosheets has been grown on the primary N-TiO_2 nanotubes, coinciding with the results from the SEM observation.

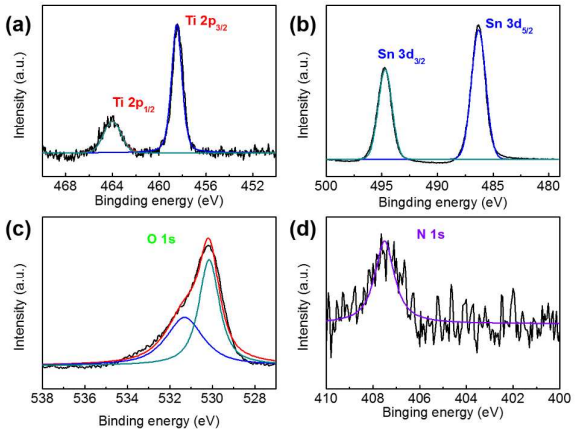

Fig. 4 XPS spectra of (a) Ti 2p (b) Sn 3d (c) O 1s (d) N 1s for the Sn_3O_4/N-TiO_2 hierarchical hybrid nanostructures.

The chemical composition and valence state was characterized by X-ray photoelectron spectroscopy (XPS). The full range of XPS spectra of Sn_3O_4/N-TiO_2 are shown in **Fig. S7**. It shows the Sn_3O_4/N-TiO_2 hierarchical hybrid nanostructures in the range of 50-950 eV. And impurities even carbon residue were not observed in the spectra. As shown in Fig. 4a, the binding energies (BE) of Ti $2p_{3/2}$ and Ti $2p_{1/2}$ are 458.3 and 464.1 eV respectively, which are ascribed to the Ti^{4+} oxidation state.[37, 38] Fig. 4b shows the Sn $3d_{5/2}$ peak at 486.3 eV and Sn $3d_{3/2}$ peak at 494.8 eV from the Sn_3O_4 material.[14] From Fig. 4c, O 1s can be seen and it will be useful in identifying core levels. An additional peak for N-TiO_2 appeared at about 531.3 eV, which attributed to the presence of Ti-O-N bonds.[39] The formation of oxidized Ti-N led to the appearance of Ti-O-N structure and this result is coincides with the fact that the presence of oxidized nitrogen should appear at a higher binding energy (>-400eV).[40] Fig. 4d shows the N 1s XPS spectra of the pristine and the N-doped TiO_2 nanotubes. Only one N 1s peaks at 407.5 eV are present in the spectra of N-doped samples.[41]

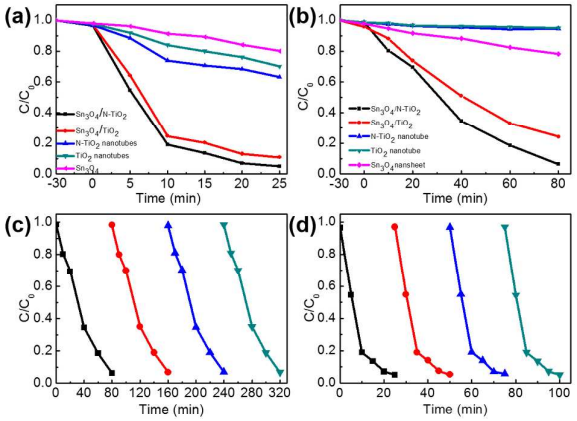

Fig. 5 Photocatalytic degradation of MO in the presence of TiO_2 nanotubes, Sn_3O_4 nanosheets, Sn_3O_4/TiO_2 and Sn_3O_4/N (5%)-TiO_2 (mole ratio N-TiO_2:Sn_3O_4 = 2:1) hierarchical hybrid nanostructures under either (a) UV or (b) visible light irradiation. And photocatalytic degradation of MO by Sn_3O_4/N-TiO_2 hierarchical hybrid nanostructure in repeated experiments under (c) visible and (d) UV light irradiation.

Fig. 5 The photodegradation of MO under UV and visible light irradiation were used to evaluate the photocatalytic performance of catalysts. In the experiments, pure TiO_2 nanotubes, N-TiO_2 nanotubes and pure Sn_3O_4 nanosheets were used as a photocatalytic reference to study the photocatalytic activity of the Sn_3O_4/N (5%)-TiO_2 (mole ratio N-TiO_2:Sn_3O_4 = 2:1) hierarchical nanostructures. Fig. S8 showed a control experiments performed under different conditions: (1) UV or visible light irradiation but in the absence of the photocatalysts, and (2) in the presence of photocatalysts but in the dark. The result of Fig. S8 indicated that no degradation effect can be checked out if there is no light in the photocatalyst contained system or if there is no photocatalyst in the experimental system under light irradiation. Fig. 5a shows the degradation curves of MO on the pure TiO_2 nanotubes, N-TiO_2 nanotubes, Sn_3O_4 nanosheets, Sn_3O_4/TiO_2 and Sn_3O_4/N-TiO_2 hierarchical nanostructures under UV irradiation.Within 25 min, for the pure TiO_2 nanotubes, about 30% of MO is degraded. For N-TiO_2, the degradation ratio is about 37%. For Sn_3O_4, is only about 20%. Surprisingly, for the Sn_3O_4/TiO_2 hierarchical nanostructures, about 90% of MO can be degraded. And for the Sn_3O_4/N-TiO_2 hierarchical nanostructures, the photocatalytic performance is significantly improved and MO can be completely degraded within 25 mins. As mentioned above, Sn_3O_4 is not a good UV active photocatalyst, the enhanced UV photocatalysis activity of Sn_3O_4/N-TiO_2 nanotube composites should be contributed to the hybrid nanostructures of Sn_3O_4 and N-TiO_2. Under visible light irradiation (Fig. 5b), TiO_2 nanotubes and N-TiO_2 nanotubes had no photocatalytic activity within 80 mins, except for the decent adsorption of MO. Meanwhile, Sn_3O_4 nanosheets exhibited negligible photocatalytic activity and the photodegradation efficiency of MO just reached about 22% after 80 min of reaction. In comparison, 76% of MO is photocatalytically degraded by Sn_3O_4/TiO_2 and 95% of MO is photocatalytically degraded by Sn_3O_4/N-TiO_2. Comparison of the photocatalytic activities of the Sn_3O_4/TiO_2 hierarchical hybrid nanostructures at different mole ratios of TiO_2 and Sn_3O_4 and at different content of N under either (a) visible or (b) UV light irradiation are shown in the Fig. S9 and Fig. S10.

To examine the photocatalytic stability of the catalysts, the efficiency of the MO photodegradation was evaluated in a repetitive mode using with the same photocatalysts. As shown in Fig. 5c and d, the MO dye was quickly decomposed after every injection of the MO solution and the Sn_3O_4/N-TiO_2 nanotube hybrid nanostructures is stable under repeated experiments with a nearly constant photodecomposition rate. Thus, the Sn_3O_4/N-TiO_2 nanotube hybrid nanostructure is an effective and stable photocatalyst under UV and visible light irradiation.

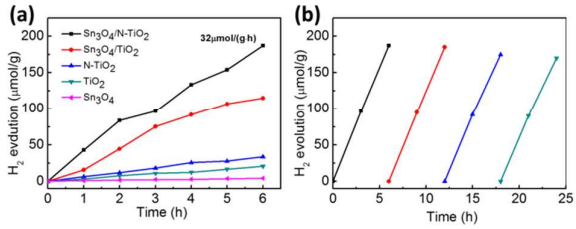

Fig. 6 (a) Photocatalytic H_2 evolution from the aqueous methanol solution over TiO_2 nanotubes, N-TiO_2 nanotubes, Sn_3O_4 nanosheets, Sn_3O_4/TiO_2 and Sn_3O_4/N-TiO_2 hierarchical hybrid nanostructures. (b) Photocatalytic H_2 evolution in 6 h repeated cycles by the Sn_3O_4/N (5%) -TiO_2 (mole ratio N-TiO_2:Sn_3O_4 = 3:1) hierarchical hybrid nanostructures.

To further demonstrate the enhanced photocatalytic property of the Sn_3O_4/N-TiO_2 hierarchical hybrid nanostructure, the evolution of hydrogen was measured according to the photocatalytic water-splitting process. As shown in Fig. 6, the amount of hydrogen increases linearly with the irradiation time during 6 h for TiO_2 nanotubes, N-TiO_2 nanotubes, Sn_3O_4 nanosheets, Sn_3O_4/TiO_2 and Sn_3O_4/N (5%) -TiO_2 (mole ratio N-TiO_2:Sn_3O_4 = 3:1) hierarchical hybrid nanostructures. The hydrogen generation rate of the Sn_3O_4/N-TiO_2 hierarchical hybrid nanostructure is about 32 μmol/h/g, while the hydrogen generation rate of the Sn_3O_4/TiO_2 and N-TiO_2 nanotubes is about 19 μmol/h/g and 5.5 μmol/h/g, respectively. Neither the TiO_2 nor the Sn_3O_4 materials exhibited obvious H_2 evolution. These results indicated that the Sn_3O_4/N-TiO_2 hierarchical hybrid nanostructure has the highest photocatalytic activity among these materials. Photocatalytic H_2 evolution from the aqueous methanol solution for Sn_3O_4/N-TiO_2 hierarchical hybrid nanostructure at different ratios are shown in the Fig. S11. More importantly, after four cycles of 6 h reaction, the Sn_3O_4/N-TiO_2 hierarchical hybrid nanostructures still retained high photocatalytic activity, which demonstrates the stability of them (**Fig. 6b**).

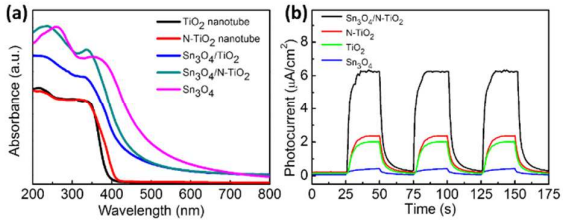

Fig. 7 (a) UV-Vis diffuse reflectance spectra of pure TiO_2 nanotubes, N-TiO_2 nanotubes, Sn_3O_4 nanosheets, Sn_3O_4/TiO_2 hierarchical hybrid

nanostructures, and Sn_3O_4/N-TiO_2 hierarchical hybrid nanostructures. **(b)** Photocurrent response for N-TiO_2 nanotube, Sn_3O_4 nanosheets and Sn_3O_4/N-TiO_2 under 0.1V bias.

Fig. 7a shows the UV-Vis diffuse reflectance spectra of TiO_2 nanotubes, N-TiO_2 nanotubes, Sn_3O_4 nanosheets, Sn_3O_4/TiO_2 hierarchical hybrid nanostructures, and Sn_3O_4/N-TiO_2 hierarchical hybrid nanostructures. The UV-vis spectra of TiO_2 can be used to explain the enhancement of the photocatalytic properties of the hybrid nanostructure under visible light. The spectrum of TiO_2 nanotubes exhibited the typical absorption behaviour of a wide-band-gap oxide semiconductor, which has an intense absorption band with a steep edge at about 380 nm (the band gap is about 3.26 eV). N-TiO_2 have an absorption band edge at about 400 nm (the band gap is about 2.97 eV). The band gap of the pure Sn_3O_4 nanosheet was calculated to be about 2.38 eV. The band gap of Sn_3O_4/N-TiO_2 hybrid nanostructures ranged from 2.69 eV to 2.48 eV and decreased as the molar ratio of N-TiO_2: Sn_3O_4 increasing from 4:1 to 1:1(see Fig. S13). The red shift of absorption band edge should lead to a better photocatalytic efficiency, especially under visible-light irradiation.[42] It was observed that the pale yellow product exhibited strong absorption in the UV range and had little absorbance in the visible range.

To further explain the enhancement of photocatalytic property of Sn_3O_4/N-TiO_2 hierarchical hybrid nanostructures catalyst, photoelectochemistry performance of TiO_2 nanotube, N-TiO_2 nanotube, Sn_3O_4 nanosheet and Sn_3O_4/N-TiO_2 were measured under 0.1 V bias. Fig. 7b shows the I-t measurements to examine the photoresponse of the samples over cycles of light on-off under 0.1V bias. When the irradiation was interrupted, the photocurrent rapidly dropped to almost zero (steady-state value), and the photocurrent reverted to its original value once light was switched on again.[43] The photocurrent of theTiO_2 nanotube and N-TiO_2 nanotube anode is about 2 μA/cm^2 and 2.15 μA/cm^2, the photocurrent of the Sn_3O_4 nanosheet anode is about 0.3 μA/cm^2, while the photocurrent of the Sn_3O_4/N-TiO_2 hierarchical hybrid nanostructures anode approaches 6.3 μA/cm^2, which is almost 3 times as that of N-TiO_2 nanotube anode. The significant photocurrent enhancement was ascribed to the improved charge separation of Sn_3O_4/N-TiO_2 heterojunction structure.

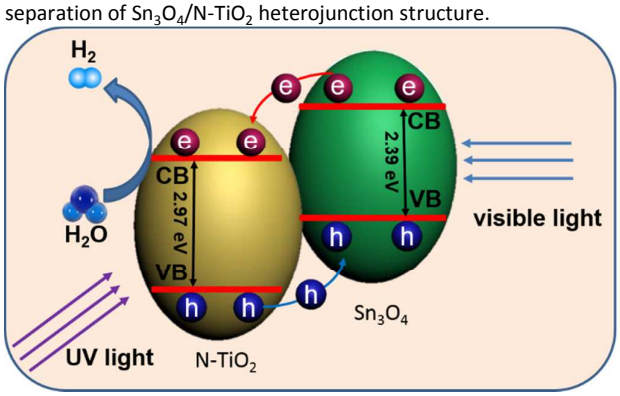

Scheme. 1 Illustration of photo-induced charge transferring and separation at the interface of Sn_3O_4/N-TiO_2 hierarchical hybrid nanostructures.

Based on the above results, the photoeletrochemical water splitting mechanism is proposed in Scheme 1. When Sn_3O_4 contacts N-TiO_2 cores to form a heterojunction, the band structure of Sn_3O_4/N-TiO_2 shells is reconfigured. The energy bands of the N-TiO_2 and Sn_3O_4 shifts upward and downward along with the diffusion of carriers until the Fermi levels of N-TiO_2 and Sn_3O_4 reach equilibrium. Under light irradiation, photogenerated holes and electrons appear in the valence bands (VB) and conduction bands (CB) of N-TiO_2 and Sn_3O_4, respectively. Due to the band position of N-TiO_2 and Sn_3O_4, the photogenerated electrons in Sn_3O_4 CB were easily injected into TiO_2 CB, meanwhile the photogenerated holes in TiO_2 VB were injected into Sn_3O_4 VB. In addition, the morphology of Sn_3O_4/N-TiO_2 seems as a special Junes system, the photogenerated holes in N-TiO_2, the minority carrier, had a very short migration distance to Sn_3O_4 due to the thin N-TiO_2 nanotube wall (20 nm) as mentioned before. So, photogenerated electrons have a very small chance to recombine with holes. Furthermore, the inner surface of N-TiO_2 is an open tube, so electrons can be consumed to achieve chemical reduction reaction for H_2 evolution at these sites. Meanwhile, the thin N-TiO_2 nanotube wall also arise short migration distance for electrons. Therefore, the electrons in TiO_2 CB which not only came from TiO_2 UV irradiation, but also Sn_3O_4 injection, had a high chance to contribute the reduction reaction. In one word, for our hybrid photocatalyst, the photogenerated electron–hole pairs are effectively separated, under the synergistic effects between band structures and morphology, which is crucial for the enhancement of photocatalytic activity. We believe that the combined effects of the introduction of N and the formation of the Sn_3O_4/N-TiO_2 heterojunction contribute to the enhancement in the efficiency of photocatalytic activity.

Experimental

Materials

All the reagents in this work are analytic grade and commercially available. Tetrabutyl titanate ($Ti(OC_4H_9)_4$), Tin(II) chloride dehydrate ($SnCl_2{\cdot}2H_2O$), NaOH, acetic acid, acetylacetone, trisodium citrate dehydrate, methyl orange and urea were purchased from China National Medicines Corporation Ltd, and the polyvinylpyrrolidone (PVP, Mw = 1300000) were purchased from Sigma Aldrich. All the chemicals were used as received without further purification.

Synthesis

Preparation of N-doped TiO_2 nanotubes

Firstly, 1.05 g polyvinylpyrrolidone powder (PVP, Mw = 1300000) was added to a mixture of 6.0 g absolute ethanol and 19 g acetic acid in a capped bottle. The obtained solution was stirred for 1 h to generate a homogeneous solution. Then 14.85 g $Ti(OC_4H_9)_4$ and 3.0 g acetyl acetone was added to the solution, and the mixture was continuously stirred for another 1 h to make a precursor solution. 12.5 g mechanical pump oil was added to the solution, and the mixture was continuously stirred for 12 h. Then 1 mL of the solution was placed in a 5 mL syringe equipped with a blunt metal needle of 0.8 mm diameter. A stainless steel plate covered with a sheet of aluminium foil was employed as the collector. The distance between the needle tip and collector was 25 cm, and the voltage was set at 22 kV. The as-collected nanotubes were calcined at 500 ℃ for 2 h to form anatase TiO_2 nanotubes. The detailed

experimental conditions for the fabrication of N5%, N10%, N15%, and N20% are listed in table S1.

Fabrication of Sn_3O_4/N-TiO_2 hierarchical nanostructures

In a typical experiment, 0.016 g N-TiO_2 nanotubes， 0.27 g $SnCl_2{\cdot}2H_2O$ and 0.882 g $Na_3C_6H_5O_7{\cdot}2H_2O$ were dissolved in 50 mL of deionized water under magnetic stirring, respectively. The solution adjusted to pH =5.5 with NaOH. Then the resulted clear solution was transferred into a 100 mL Teflon-lined stainless steel autoclave, which was heated to 180℃ and maintained for 12 h. Then, the autoclave was cooled down to room temperature. The obtained composite nanotubes were washed with deionized water and ethanol to remove any ionic residual, then dried in an oven at 80℃ for 4 h. The as-fabricated sample was denoted as Sn_3O_4/N-TiO_2. By turning the precursor concentration for synthesizing Sn_3O_4, three other samples of Sn_3O_4/N-TiO_2 were fabricated. And Sn_3O_4 was synthesized in the absence of TiO_2 nanotube. The detailed experimental conditions for the fabrication of 1:1, 2:1, 3:1 and 4:1 are listed in table. S1.

Materials Characterization

XRD pattern of the samples were recorded by X-ray diffraction spectrometer with Cu Kα radiation (D8-advance, BrukerAXS, Germany).

The morphology and microstructure of the samples were examined by SEM-a HITACHI S-8020 microscopy. The composition of N-TiO_2 was analysed by an energy-dispersion spectroscopy (EDS, Oxford link system) analyser, which was equipped to the SEM.

The TEM images were acquired on a JEOL JEM 2100 microscope with an operating voltage of 200 kV. The sample for TEM was prepared by dropping a methanol suspension of the sample powder onto a copper microgrid. The sample was thoroughly dried in vacuum prior to observation.

Photocatalytic test: The photocatalytic activity of Sn_3O_4/TiO_2 was assessed by the photodegradation of MO on a photochemical reaction apparatus. In a typical experiment, 20 mL aqueous suspensions of MO (20 mg/L) and 40 mg of sample were placed in a 50 mL beaker. Prior to irradiation, the suspensions were magnetically stirred in the dark for 30 min to establish adsorption/desorption equilibrium between the dye and the surface of the catalyst at room temperature. A 300 W mercury lamp with a maximum emission of 356 nm was used as the UV light source and a 350 W Xe lamp with a cut-off filter (λ > 420 nm) was used as the visible light source. For comparison, photodegradation abilities of 40 mg TiO_2 nanotubes and 40 mg Sn_3O_4 nanosheets were evaluated under the same experimental conditions. At varied irradiation time intervals, the residual MO concentration in the supernatant was analyzed by UV-Vis spectroscopic measurement (Shimadzu UV-3600). Four consecutive cycles were tested. The samples were washed thoroughly with water and dried after each cycle.

UV-vis diffuse reflectance spectra (DRS) of the samples were recorded on a UV-vis spectrophotometer (UV-3600, Shimadzu) with an integrating sphere attachment within the range of 200 to 800 nm and with $BaSO_4$ as the reflectance standard.

The H_2 evolution experiments were carried out in a gas-closed circulation system. In a typical reaction, the 100 mg catalyst powder was dispersed in CH_3OH aqueous solution using a magnetic stirrer (80 mL of distilled water + 20 mL of CH_3OH). A commercial solar simulator (300W) equipped with a Xenon lamp as the light source for photocatalytic H_2 generation. The power density of the incident light was about 100 mW/cm^2. The H_2 evolution was measured with an on-line gas chromatograph (GC-7900).

Photoelectrode fabrication: 50 mg of photocatalyt sample was mixed with 20 ml of terpineol and stirred with a magnetic stirrer for 10 h. The suspension was dip-coated onto the fluorine-doped tin oxide (FTO) glass substrate. A doctor blading technique was employed to ensure the same thickness for each photoelectrode. The photoelectrode was dried on a hot plate at 80 ^oC, and then heated in a quartz tubular furnace in Ar at 200 ^oC for 2 h. Digital pictures of the N-TiO_2, Sn_3O_4, Sn_3O_4/N-TiO_2 anode are shown in Fig. S9. A Cu wire was connected to the FTO substrate with the silver colloid paste. Finally, epoxy was solidified to cover the FTO substrate, the silver paste and the Cu wire to avoid short current in the measurement.

Photoelectrochemical measurement: photoelectrochemical analyses were carried out using a standard three-electrode cell with Ag/AgCl as reference electrode and Pt sheet as the counter electrode in the KCl solution (1M). The electrolyte was bubbled with N_2 for 2 h to remove O_2. The light source used was identical with that used in the photocatalytic H_2 generation testing.

In situ XPS analysis: In the present work, visible light irradiation was carried out in XPS preparation chamber, and the sample was then transferred to XPS analysis chamber without being exposed to the air. This “in situ” setting makes it possible to eliminate the influence of environmental pollutions, thereby permitting the detection of the intrinsic surface reaction under visible light irradiation. A Mercury–Xenon lamp (LC8, HAMAMATSU, 200 W, Japan) with 420 and 800 nm cutoff filters was used as an excitation light source, and introduced into the XPS preparation chamber though a sapphire window. Prior to the illumination of the sample, CH_3OH was adsorbed onto the surface of the sample by vacuum drying of the suspension. After the irradiation in XPS preparation chamber, the photoinduced holes were quenched by the photocatalytic oxidation of CH_3OH, whereas photoexcited electrons remained in Sn_3O_4. Thus, the differential spectrum between before and after irradiation was attributed to the electrons in Sn_3O_4.

Conclusions

In summary, to our best knowledge， the Sn_3O_4/N-TiO_2 hierarchical hybrid nanostructures with novel architectures were successfully fabricated for the first time using the solvothermal process and electrospinning technology. Comparing to the pure TiO_2 nanotubes, Sn_3O_4 nanosheets, N-TiO_2 nanotubes and Sn_3O_4/TiO_2, the Sn_3O_4/N-TiO_2 hierarchical hybrid nanostructures exhibited a high photocatalytic performance for the decomposition of MO and water splitting. These results indicated that the Sn_3O_4/N-TiO_2 hierarchical hybrid nanostructure is promising candidate material for wastewater treatment and hydrogen evolution.

Acknowledgements

Thanks to Dr. Weiwei Wu (Technion-Israel Institute of Technology) for teaching the electrospinning technology and revise the

manuscript writing. The authors thankful for funding from the National Natural Science Foundation of China (Grant No.51402063), China Postdoctoral Science Foundation (2014M550673), and the "100 Talents Program" of the Chinese Academy of Sciences. Thanks for the support from the "thousands talents" program for pioneer researcher and his innovation team, China.

Notes and references

1 X. Chen, S. Shen, L. Guo and S. S. Mao, *Chemical Reviews*, 2010, 110, 6503-6570.
2 N. Serpone and A. Emeline, *The Journal of Physical Chemistry Letters*, 2012, 3, 673-677.
3 N. Ren, J. Li, J. Qiu, Y. Sang, H. Jiang, R. I. Boughton, L. Huang, W. Huang and H. Liu, *Small*, 2014, 10, 3169-3180.
4 W. Zhou, H. Liu, R. I. Boughton, G. Du, J. Lin, J. Wang and D. Liu, *J Mater Chem*, 2010, 20, 5993-6008.
5 J. Tian, Z. Zhao, A. Kumar, R. I. Boughton and H. Liu, *Chemical Society Reviews*, 2014, 43, 6920-6937.
6 S. G. Kumar and L. G. Devi, *The Journal of Physical Chemistry A*, 2011, 115, 13211-13241.
7 Z. Zhao, J. Tian, Y. Sang, A. Cabot and H. Liu, *Adv Mater*, 2015, 27, 2557-2582.
8 Y. Sang, Z. Zhao, J. Tian, P. Hao, H. Jiang, H. Liu and J. P. Claverie, *Small*, 2014, 10, 3775-3782.
9 I. Paramasivam, H. Jha, N. Liu and P. Schmuki, *Small*, 2012, 8, 3073-3103.
10 S. D. Sharma, D. Singh, K. Saini, C. Kant, V. Sharma, S. Jain and C. Sharma, *Applied Catalysis A: General*, 2006, 314, 40-46.
11 Z. Xiong and X. S. Zhao, *Journal of the American Chemical Society*, 2012, 134, 5754-5757.
12 S. Klosek and D. Raftery, *The Journal of Physical Chemistry B*, 2001, 105, 2815-2819.
13 D. Chen, Z. Jiang, J. Geng, Q. Wang and D. Yang, *Industrial & engineering chemistry research*, 2007, 46, 2741-2746.
14 M. Manikandan, T. Tanabe, P. Li, S. Ueda, G. V. Ramesh, R. Kodiyath, J. Wang, T. Hara, A. Dakshanamoorthy and S. Ishihara, *Acs Appl Mater Inter*, 2014, 6, 3790-3793.
15 Y. He, D. Li, J. Chen, Y. Shao, J. Xian, X. Zheng and P. Wang, *RSC Adv.*, 2013, 4, 1266-1269.
16 J. Lin, J. Shen, R. Wang, J. Cui, W. Zhou, P. Hu, D. Liu, H. Liu, J. Wang and R. I. Boughton, *J Mater Chem*, 2011, 21, 5106-5113.
17 S. J. Hong, S. Lee, J. S. Jang and J. S. Lee, *Energ Environ Sci*, 2011, 4, 1781-1787.
18 Z. Zhao, H. Liu and S. Chen, *Nanoscale*, 2012, 4, 7301-7308.
19 J. Zhu and M. Zäch, *Current Opinion in Colloid & Interface Science*, 2009, 14, 260-269.
20 S. M. Gupta and M. Tripathi, *Chinese Science Bulletin*, 2011, 56, 1639-1657.
21 N. Bao, L. Shen, T. Takata and K. Domen, *Chemistry of Materials*, 2007, 20, 110-117.
22 N. Li, G. Liu, C. Zhen, F. Li, L. Zhang and H. M. Cheng, *Advanced Functional Materials*, 2011, 21, 1717-1722.
23 W. Zhou, Z. Yin, Y. Du, X. Huang, Z. Zeng, Z. Fan, H. Liu, J. Wang and H. Zhang, *Small*, 2013, 9, 140-147.
24 Y. Wang, L. Zhang, K. Deng, X. Chen and Z. Zou, *The Journal of Physical Chemistry C*, 2007, 111, 2709-2714.
25 J. Jitputti, Y. Suzuki and S. Yoshikawa, *Catalysis Communications*, 2008, 9, 1265-1271.
26 X. Yu, X. Han, Z. Zhao, J. Zhang, W. Guo, C. Pan, A. Li, H. Liu and Z. L. Wang, *Nano Energy*, 2015, 11, 19-27.
27 H. Xu, S. Ouyang, L. Liu, P. Reunchan, N. Umezawa and J. Ye, *Journal of Materials Chemistry A*, 2014, 2, 12632-12661.
28 H. Kato, K. Asakura and A. Kudo, *Journal of the American Chemical Society*, 2003, 125, 3082-3089.
29 Y. Su, Z. Wu, Y. Wu, J. Yu, L. Sun and C. Lin, *Journal of Materials Chemistry A*, 2015, 3, 8537-8544.
30 P. Zhong, X. Ma, X. Chen, R. Chen. R. Zhong, X. Liu, D. Ma, M. Zhang and Z. Li, *Nano Energy* 2015, 16, 99-111.
31 V. Augugliaro, G. Camera-Roda, V. Loddo, G. Palmisano, L. Palmisano, J. Soria and S. Yurdakal, *The Journal of Physical Chemistry Letters*, 2015, 6, 1968-1981.
32 W. Jia, Y. Guan, D. Wang, X. Zhang, D. Liu, H. Jiang, J. Wang, X. Liu, H. Liu and S. Chen, *Chemistry an Asian Journal*, 2014, 9, 1648-1654.
33 T. Jiang, C. Jia, L. Zhang, S. He, Y. Sang, H. Li, Y. Li, X. Xu and H. Liu, *Nanoscale*, 2015, 7, 209-217.
34 J. Pan, Y. Sheng, J. Zhang, J. Wei, P. Huang, X. Zhang and B. Feng, *Journal of Materials Chemistry A*, 2014, 2, 18082-18086.
35 G. Chen, S. Ji, Y. Sang, S. Chang, Y. Wang, P. Hao, J. P. Claverie, H. Liu and G. Yu, *Nanoscale*, 2015, 7, 3117-3125.
36 X. Yu, J. Zhang, Z. Zhao, W. Guo, J. Qiu, X. Mou, A. Li, J. P. Claveria and H. Liu, *Nano Energy*, 2015, 16, 207-217.
37 W. Ren, Z. Ai, F. Jia, L. Zhang, X. Fan and Z. Zou, *Applied Catalysis B: Environmental*, 2007, 69, 138-144.
38 Y. Xin, L. Wu, L. Ge, C. Han, Y. Li and S. Fang, *Journal of Materials Chemistry A*, 2015, 3, 8659-8666.
39 G. Battiston, R. Gerbasi, A. Gregori, M. Porchia, S. Cattarin and G. Rizzi, *Thin Solid Films*, 2000, 371, 126-131.
40 V. J. Babu, M. K. Kumar, A. S. Nair, T. L. Kheng, S. I. Allakhverdiev and S. Ramakrishna, *international journal of hydrogen energy*, 2012, 37, 8897-8904.
41 A. Christie, J. Lee, I. Sutherland and J. Walls, *Applications of surface science*, 1983, 15, 224-237.
42 L. Jing, H. Tan, R. Amal, Y. Nq and K. Sun, *Journal of Materials Chemistry A*, 2015, 3, 15675-15682.
43 Y. Sang, Z. Zhao, M. Zhao, P. Hao, Y. Leng and H. Liu, *Advanced Materials,* 2015, 27, 363-369.